Comparative study of numerical modelling and experimental investigation for vessel-docking operations

Xueliang Wen [a], Jianan Zhang [a], Muk Chen Ong [a], Aleksander Kniat [b],*

[a] *Department of Mechanical and Structural Engineering and Materials Science, University of Stavanger, Stavanger, Norway*
[b] *Faculty of Mechanical Engineering and Ship Technology, Gdańsk University of Technology, Gdańsk, Poland*

ARTICLE INFO	ABSTRACT
	A comparative study between numerical modelling and experimental investigation is performed to validate the developed numerical method for simulating floating dock operations with a vessel on board. Both model-scale and full-scale experimental tests are performed on floating docks with a vessel on board, and the draughts using draught meters, floating positions and bending of the floating dock are measured. The present numerical method is proposed based on a quasi-static assumption during vessel-docking operations. A static analysis model is built to determine the static response of a floating dock under a specific ballast water distribution based on a hydrostatic force model and a Newton-Raphson method. A bending model is proposed to calculate the deflection of the floating dock along the longitudinal direction. Results of the mode-scale tests show that the draught measurements and the floating positions of the dock and vessel predicted using the present numerical method agree well with the corresponding experimental results. It proves the accuracy of the present numerical method for simulating vessel-docking operations. Moreover, a well-designed ballast plan enables successful de-ballasting operations on the model-scale dock, even in the event of one to three pump failures. The comparison of the deflection changes of the floating dock in the field test measurements further proves the accuracy of the present bending model. Therefore, the validated numerical model tested on both model-scale and full-scale docks provides a reliable foundation for creating digital twin of floating docks in shipyards.

1. Introduction

The number and size of new vessels have risen sharply in recent years. To keep up with the demand for new vessels, dry docks have been built in the shipyards to increase the capacities for ship construction, repair and maintenance Warnke, 1975 [1]. A dry dock is a narrow basin or vessel which can be flooded to allow a vessel to be floated in and then drained to allow the vessel to rest on a dry platform. There are two main types of dry docks (see Fig. 1): graving docks and floating docks. A graving dock is a fixed basin built into the ground near the sea [2] and closed by gates. When the gates are opened, a vessel is floating inside the dock. Then, the gates are closed, and the water is pumped out, leaving the vessel supported on the docking blocks for being inspected or serviced. In contrast, the floating docks are commonly operated in sheltered harbours, not occupying the space on land. They are designed in a "U" shape, with a pontoon as the bottom horizontal part and two wing walls as the vertical sides. Multiple ballast tanks are equipped inside the pontoon

---

and two wing walls. The position of the floating docks can be adjusted by ballasting or de-ballasting so that the docked vessel can be lifted during the de-ballasting operations. In recent years, floating docks have become an alternative to graving docks due to the efficiency in construction and flexibility in operations.

The ballasting and de-ballasting operations involve filling and emptying sea water in the ballast tanks and transferring water among them to achieve the desired floating position of the dock. These tasks are typically carried out manually by a skilled dock master through controlling ballast valves and pumps. The docking process lasts for hours, and the dock and the vessel move slowly and steadily. However, potential risks still exist during the operational conditions, such as malfunctions of the ballast water system [5–11], overloading [12], and improper ballast control [13]. These risks pose safety challenges during floating dock operations.

To address these challenges, developing a digital twin for vessel-docking operations is a potential solution. A digital twin is a digital representation of a physical object, based on sensor data and high-fidelity simulations [14]. It can describe the current state of the physical object, predict the future state [15], and offer optimization strategies for decision-making by detecting potential problems [16]. Implementing a digital twin of the floating docks allows real-time monitoring of dock and vessel status, enhancing operational safety and assisting decision-making for the dock masters [17] during floating dock operations.

The construction of a digital twin includes modelling, data fusion, data interaction and collaboration, as well as service [18]. Therefore, it is crucial to monitor the real-time responses of the floating docks during floating dock operations. Recent advances in sensor application can be adopted. For instance, Korotaev et al. [19] developed a real-time measuring system using camera-based devices to obtain a floating dock's deflection. Laboratory tests on a model-scale dock and field tests on a real dock indicated that the developed system demonstrated good measurement accuracy. Yang et al. [20] proposed a deflection and inclination measuring system for a floating dock based on the connected liquid-filled pipes. The proposed measuring system was also validated by field tests. The dock's draught and ballast water levels are typically measured using pressure and level transmitters [21,22]. Moreover, the fibre-optic strain sensors have been widely used for floating structures, such as ships [23], underwater vessels [24], floating wind turbines [25], and offshore platforms [26].

For implementing the digital twin, a comprehensive numerical model for floating dock operations is required. The results obtained from the numerical model of the floating dock need to be collected [27] and integrated with the real-time data [28]. The dynamic analysis methodology for regular vessels is inadequate for simulating floating dock operations due to the inefficiency in modelling the wave and body interaction [29]. However, for the floating dock in a sheltered area, the wave and current loads acting on the floating dock are negligible. A novel and more efficient model considering ballast water adjustment was developed by Zhang et al. [30–32]. This code aims to simulate floating dock operations in the time domain, featuring a six-degree-of-freedom (6-DOF) model, a hydro-static force model, a hydrodynamic force model, a mooring force model, a hydraulic model, and a contact force model. Additionally, an automatic ballast control strategy is incorporated to regulate the opening angles of the ballast valves, ensuring that the dock's roll and pitch angles remain within allowable ranges [31,33]. The deflection of the floating docking during the vessel-docking operation was also calculated using a bending model [31]. The hydrostatic, hydrodynamic, and mooring force models were verified against their corresponding results obtained using various software and models, including theoretical models, HydroD, Autodesk Inventor, lumped-mass model and Code-Aster. To prove the reliability of this code, further validations through experimental tests are necessary. Zhang et al. [32] performed a comparative study of the numerically calculated and experimentally measured static responses of a model-scale floating dock with a ratio of 1/70. They conducted various cases of the single floating dock with different ballast water distributions. However, the docked vessel was not involved. To validate the accuracy of simulating vessel-docking operations, experiments involving floating docks with vessels on board are required.

Motivated by this, model-scale experiments and field test measurements are performed on floating docks with vessels on board in this study. The floating dock's draughts and floating positions recorded in the model-scale tests are compared with the predictions using the static analysis model proposed by Zhang et al. [32]. The deflection changes in the floating dock in the full-scale experiments are compared with the predictions using the bending model by Zhang et al. [31]. The present study is organized as follows. The static analysis model, hydrodynamic force model and bending model are described in Section 2. The results of the model-scale and full-scale

(a) Graving dock   (b) Floating dock

Fig. 1. Graving dock in Charlestown Navy Yard [3] and floating dock at Myklebust Verft AS [4].

experiments and the corresponding numerical simulations are performed in Sections 3 and 4, respectively. Finally, the conclusions are summarized in Section 5.

2. Methodology

An in-house code was developed by Zhang et al. [32] for simulating floating dock operations, enabling the static analysis of floating dock operations and facilitating the determination of the floating dock's static equilibrium position. The code was proposed based on a quasi-static assumption that the floating dock remains static at each draught despite changes in the distribution of ballast water. The floating position of the floating dock under any specific ballast water distribution can be obtained using the present static analysis model.

2.1. Static analysis model

The static analysis model, proposed by Zhang et al. [32], is used to calculate the static response of a single floating dock with a specific distribution of the ballast water. In the present study, the vessel is considered during operations. Fig. 2 shows the body-fixed and coordinate systems of the floating dock. The body-fixed coordinate system $oxyz$ moves with the floating dock, where the origin is located at the centroid of the dock's bottom, the x-axis points from the aft to the fore along the centreline of the bottom, the y-axis points from the starboard to the port and the z-axis point vertically upwards. The global coordinate system initially aligns with the body-fixed coordinate system. As the dock moves, the body-fixed coordinate system moves accordingly, resulting in the difference between the two coordinate systems, as shown in Fig. 2.

The governing equations for determining the floating dock's static equilibrium position with considering the vessel on board are Equations (1)–(3). These equations mean that the hydrostatic force and moments of the floating dock with a vessel on board are equal to zero at the equilibrium floating position.

$$F = F_d + F_v - (m_d + m_b + m_v)g = 0 \tag{1}$$

$$M_x = M_{d,x} + M_{v,x} - M_{b,x} = 0 \tag{2}$$

$$M_y = M_{d,y} + M_{v,y} - M_{b,y} = 0 \tag{3}$$

Here, g is the gravitational acceleration of water, m_d, m_v and m_b are the mass of the dock, vessel and ballast water, respectively. F_d and F_v represent the buoyancy forces acting on the dock and the vessel, respectively. $M_{d,x}$ and $M_{d,y}$ denote the buoyancy moments acting on the floating dock about the x- and y-axes. $M_{v,x}$ and $M_{v,y}$ are the buoyancy moments acting on the vessel about the x- and y-axes. $M_{b,x}$ and $M_{b,y}$ represent the moments about the x- and y-axes due to the gravity of the ballast water. The mass of the ballast water and the dock's buoyancy force and moments can be calculated using the hydrostatic force model described in Section 2.2.

These static equilibrium equations are solved using the Newton-Raphson method, as shown in Equations (4)–(6).

$$d^{(j+1)} = d^{(j)} - \frac{F_z}{C_{33}} \tag{4}$$

$$\gamma^{(j+1)} = \gamma^{(j)} - \frac{M_x}{C_{44}} \tag{5}$$

$$\psi^{(j+1)} = \psi^{(j)} - \frac{M_y}{C_{55}} \tag{6}$$

where j represents the index of iteration, and $C_{33} = \rho g A_w$, $C_{44} = \rho g \nabla GM_t$ and $C_{55} = \rho g \nabla GM_l$ are the restoring hydrostatic coefficients in heave, roll and pitch motions for the floating dock with a vessel on board, respectively. d is the avrage draught of the floating dock, γ and ψ are the heel and trim of the floating dock, respectively. ρ is the density of water, A_w is the water plane area, ∇ is the displaced
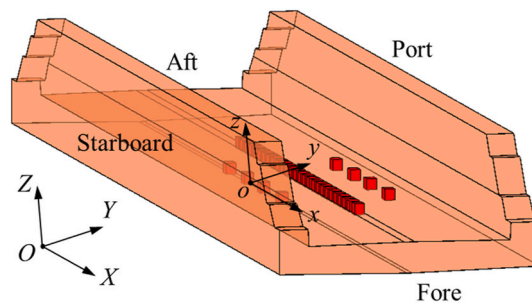

Fig. 2. Descriptions of the global and body-fixed coordinate systems of the floating docks.

volume, GM_t and GM_l are the transverse and longitudinal metacentric heights, respectively. The restoring hydrostatic coefficients are calculated based on the area and second moments of inertia for the horizonal sections of the floating dock with a vessel onboard. In this case, the floating dock and the docked vessel are considered as a single rigid body, with a vertical distance of 6.2 m between their bottoms (full scale model). The coefficients are a combination of those for the floating dock and the docked vessel. The dock's equilibrium floating position is determined when $\left|\left[d^{(j+1)} - d^{(j)}\right]/d^{(j+1)}\right|$, $\left|\left[\gamma^{(j+1)} - \gamma^{(j)}\right]/\gamma^{(j+1)}\right|$ and $\left|\left[\psi^{(j+1)} - \psi^{(j)}\right]/\psi^{(j+1)}\right|$ become smaller than a tolerance value.

2.2. Hydrostatic force model

The hydrostatic force model was proposed by Zhang et al. [30] to obtain the hydrostatic loads due to the displaced water of the floating dock and docked vessel, as well as the ballast water. The calculations are conducted based on a strip theory and Archimedes' principle. Using the strip theory, the three-dimensional (3D) force calculations are simplified as multiple two-dimensional (2D) calculations. The hydrostatic characteristics are calculated based on Archimedes' principle as shown in Equations (7)–(9). Given a water level, the geometry of each section's submerged area is expressed by $N + 1$ points and the $i - th$ point's coordinates are expressed as (x_i, y_i, z_i). The points are arranged counterclockwise. A_k is the submerged area; $y_{G,k}$ and $z_{G,k}$ are the centroid coordinates of the submerged area in y and z directions. X_{CG} and Y_{CG} are the x and y coordinates of the CoG of the floating dock or the docked vessel. ΔS_k is the thickness of the section in x direction. The hydrodynamic loads of the entire floating dock or docked vessel are obtained by integrating the hydrostatic loads of the sections along the longitudinal direction of the dock or vessel, as shown in Equations (10)–(12) [30].

$$A_k = \frac{1}{2} \sum_{i=1}^{N} (z_i + z_{i+1})(y_i - y_{i+1}) \tag{7}$$

$$y_{G,k} = \frac{1}{6A_k} \sum_{i=1}^{N} (z_{i+1} - z_i)\left(y_i^2 + y_i y_{i+1} + y_{i+1}^2\right) \tag{8}$$

$$z_{G,k} = \frac{1}{6A_k} \sum_{i=1}^{N} (y_i - y_{i+1})\left(z_i^2 + z_i z_{i+1} + z_{i+1}^2\right) \tag{9}$$

$$F_Z = \rho g \sum_{k=1}^{M} A_k \Delta S_k \tag{10}$$

$$M_X = \rho g \sum_{k=1}^{M} A_k \left(y_{G,k} - Y_{CG}\right) \Delta S_k \tag{11}$$

$$M_Y = -\rho g \sum_{k=1}^{M} A_k (x_k - X_{CG}) \Delta S_k \tag{12}$$

The water level h in each ballast tank is required to be calculated based on the amount of the water as well as the heel and trim of the floating dock. A secant method is adopted to determine the water level using an iterative formula in Equation (13) [30].

$$h^{(j+1)} = h^{(j)} - \frac{h^{(j)} - h_{pre}}{V^{(j)} - V_{pre}}\left[V^{(j)} - V_{actual}\right] \tag{13}$$

where V_{actual} is the actual ballast water volume in the current time step; h_{pre} and V_{pre} are the ballast water level and volume in the previous time step, respectively. $h^{(j)}$ and $V^{(j)}$ are the water level and the corresponding water volume in the $j - th$ iteration step, respectively.

2.3. Bending model

The bending model is a simplified structural analysis method proposed by Zhang et al. [31]. In this model, the floating dock is simplified as a 1D beam using the Euler-Bernoulli beam theory. The loads acting on the floating dock are also simplified according to the beam model. The deflection of the floating dock is calculated in Equations (14) and (15).

$$w(x_0) = -\int_0^{x_0} \int_0^{x_1} \frac{M_{bending}(x)}{EI(x)} dx dx_1 \tag{14}$$

$$w|_{x_0=0} = 0, \frac{dw}{dx}\Big|_{x_0=0} = 0 \tag{15}$$

Here $M_{\text{bending}}(x)$ and $EI(x)$ denote the dock's total bending moment and bending stiffness, respectively. The distribution of bending stiffness $EI(x)$ is given in Fig. 3. The bending stiffness was calculated based on a finite element model using Abaqus by Zhang et al. [31]. The external forces acting on the floating dock include the floating dock's buoyancy force, the gravity forces of the floating dock and the ballast water, as well as the contact force resulting from the weight of the docked vessel. The mooring forces due to the mooring lines and ropes are neglected.

3. Validation using model-scale experiment

3.1. Experiment setup and numerical modelling

The experiments took place in March 2024 in a flume tank at Gdansk University of Technology, Poland. The facilities as shown in Fig. 4 include the flume tank, the model-scale floating dock made of Polymethylmethacrylate (PMMA, commonly called plexiglass) which is the same as those used by Zhang et al. [32]. The experiments in the present study involve a model-scale vessel and ten model-scale docking blocks. The model-scale vessel with a scale ratio of 1/70 is a simplification of the docked vessel described in the study of Wen et al. [34]. Two steel plates weighing 4 kg and 8 kg respectively are positioned within the vessel to achieve the scaled mass requirements. The vessel is securely fastened to the floating dock using four elastic ropes. Fig. 5 shows the numerical model of the model-scale floating dock with a vessel on board. The specifications of the floating dock and the docked vessel are shown in Table 1. The restoring hydrostatic coefficients of the model-scale floating dock with a vessel on board are shown in Fig. 6. The restoring hydrostatic coefficients for each draught of the floating dock with a vessel on board are interpolated from the results shown in Fig. 6. The four draught meter locations can be found in Table 2, where the illustration of the four draught meters was demonstrated by Zhang et al. [32]. The draughts at the four draught meters are calculated based on the convergent results of the floating dock's draught, heel and trim. The details of the draught calculations of the four draught meters were provided by Zhang et al. [32].

The model-scale floating dock with the vessel on board is freely floating on the still water and subjected to the buoyancy force and gravitational force of the ballast water. Ballast water distributions, the draughts measured at different locations, the weight and the centre of gravity (CoG) of the empty floating dock and the vessel were recorded during the tests.

Five tests of the floating dock operations with and without malfunctioning pumps were conducted as shown in Fig. 7. The normal operation, the operations with one-pump failure and with three-pump failure are considered. The two types of failure cases correspond to the valve failure and pump failure of the full-scale floating dock, as studied by Wen et al. [34], respectively. In the present study, a specific pump is disabled during the de-ballasting operation to represent a failure scenario. The numerical models in Sections 2.1 and 2.2 will be adopted to conduct the static analyses for all these cases with various draughts. The draughts at four draught meters (see Fig. 5) are calculated for comparison with the experimental results. Visualizations of various floating positions of the floating dock are presented for comparison with the corresponding photos recorded in the experiments.

3.2. Comparison between experiment and numerical results

Fig. 8 shows the ballast water distributions at six draughts (D1-D6) in Case 1. This case is conducted for three times to show the reliability of the experimental results. In Fig. 9, the draughts obtained from four draught meters across three rounds of experiments are presented with respect to the total mass of ballast water. Three repeatable experiments were conducted, with water being pumped into the corresponding ballast tanks of the floating dock as scheduled in Fig. 8. These experiments aim to validate their repeatability, minimize human errors, and provide error bars. The maximum standard deviation of the measured draughts in these experiments is 3.2 mm, indicating acceptable repeatability. Significant variation is observed at the draught meters (a) and (d) with large draughts D5 and D6. This can be attributed to the decreased stability of the floating dock with a vessel on board, as shown in Fig. 6(a). Errors in measuring the mass distribution of the ballast water can result in more significant differences in the draughts of the four draught meters, compared to those of D1-D4, where C_{33}, C_{44} and C_{55} are much larger than those of D5-D6.

Fig. 10 shows the comparisons of the four draughts between the experimental results and the numerical predictions for Case 1. The four draught meter locations can be found in the experiment setup of Zhang et al. [32]. The error bars of the experimental results are also given. The numerical predictions can generally match the experimental results with the maximum relative error of 16 %. The error
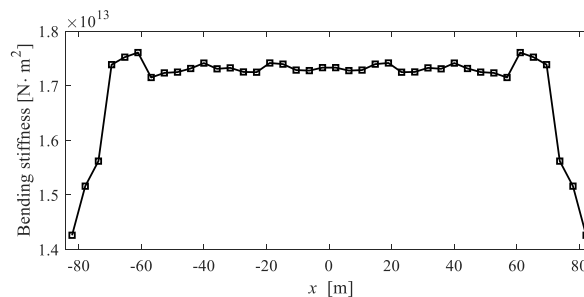

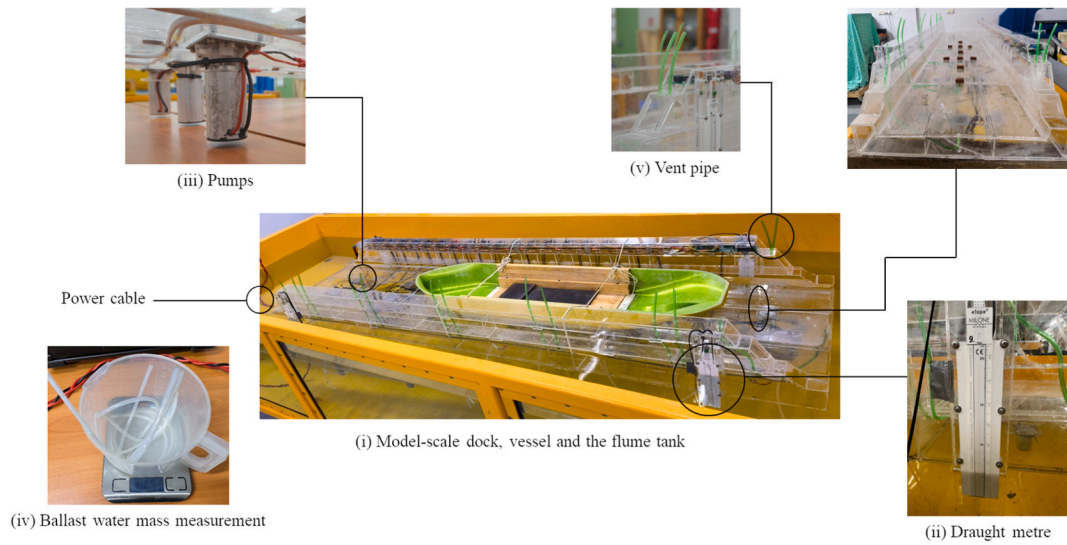**Fig. 3.** Bending stiffness along the entire dock's length [31].

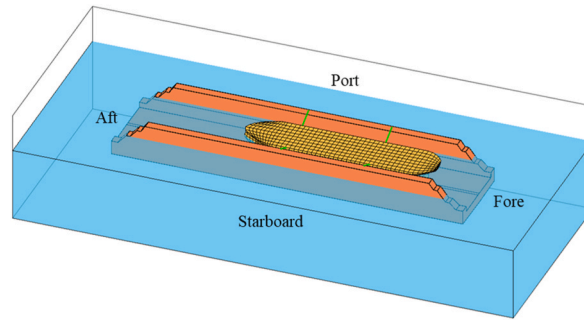**Fig. 4.** Test setup of model-scale experiments.

Fig. 5. Numerical model of the floating dock with a vessel on board.

Table 1
Floating dock and docked vessel specifications in scale model experiments.

Description	Model-scale dock	Model-scale vessel
Dimensions, $L \times B \times H$ [m]	$2.41 \times 0.57 \times 0.26$	$1.31 \times 0.288 \times 0.114$
Mass [kg]	27.8	14.8
Initial CoG, $(X_{CG0}, Y_{CG0}, Z_{CG0})$ [m]	$(0.022, 0.02065, 0.0766)$	$(0.2234, 0.0, 0.1215)$
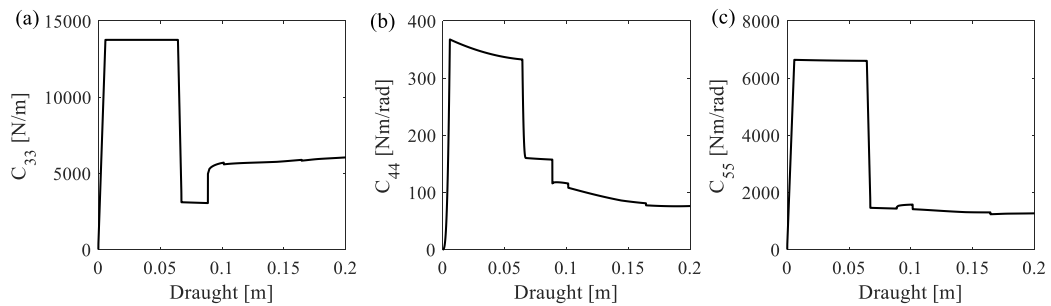
Fig. 6. Restoring hydrostatic coefficients of the model-scale floating dock with a vessel on board.

Table 2
Draught meter locations [32].

Draught meter	(a)	(b)	(c)	(d)
X [m]	−0.9345	0.9345	0.9345	−0.9345
Y [m]	−0.303	−0.303	0.303	0.303
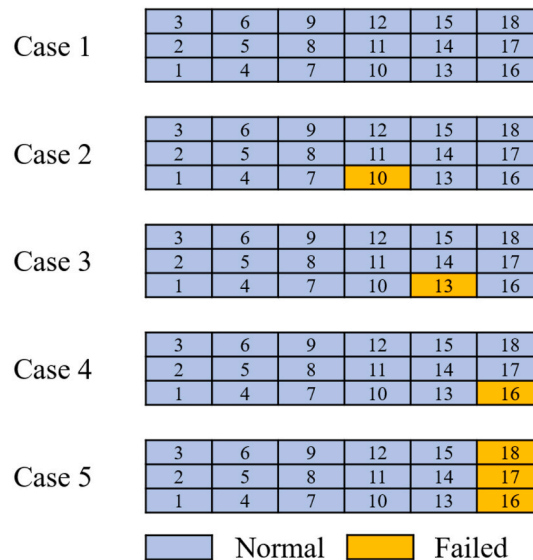
Fig. 7. Five tests of the floating dock operations with and without malfunctioning pumps.

can be attributed to the remaining ballast water that cannot be pumped out of the tanks [32]. The remaining ballast water affects the 'empty' dock's actual mass and CoG, as shown in Table 1. Fig. 11 shows the comparisons of the floating dock's and docked vessel's positions at various total masses between the experimental results and the present numerical results. The present visualizations of the numerical results are consistent with the photographs of the floating dock and the docked vessel taken in the experiments.

Fig. 12 shows the ballast water distributions at different draughts in Case 2. Throughout the vessel-docking operation, it is assumed that the pump of Tank No. 10 is malfunctioning. Consequently, the amount of ballast water in Tank No. 10 is retained during the entire de-ballasting process. The de-ballasting plan is arranged to ensure minimal heel and trim. Fig. 13 shows the comparisons of the four draughts at the draught meters between the experimental results and the numerical predictions for Case 2. A good agreement is achieved with the maximum relative error of 12 %. The entire vessel-docking process is visualized using the present numerical method. Fig. 14 shows the floating dock's and docked vessel's positions at various total mass. Compared with the normal vessel-docking operation shown in Fig. 12, the floating dock heels to the starboard and trims to the fore at the final draught due to the retained ballast water in Tank No. 10.

Fig. 15 shows the ballast water distributions at different draughts in Case 3. The pump of Tank No. 13 is assumed to be malfunctioning in this case. Fig. 16 shows the comparisons of the four draughts at the draught meters between the experimental results and the numerical predictions for Case 3. The maximum relative error is observed to be 14 %, which also exhibits good agreement between the experimental results and the numerical predictions. The visualizations of the vessel-docking process are shown in Fig. 17. The floating dock heels to the starboard and trims to the fore as it does in Case 2. The trimming is more significant than heeling because of the location of Tank No. 13.

Fig. 18 shows the ballast water distributions at different draughts in Case 4. The pump for Tank No. 16, a corner tank, is assumed to be malfunctioning. Fig. 19 shows the comparisons of the four draughts at the draught meters between the experimental results and the numerical predictions for Case 4. The agreement between the experimental results and the numerical predictions is similar to Cases 2 and 3. The maximum relative error of 12 % is observed. Fig. 20 shows the visualizations of the vessel-docking process. The floating dock significantly heels to the port at the draught of D3. Similar floating positions are also observed in Cases 2 and 3. This phenomenon is attributed to the initial CoG of the floating dock, as shown in Table 1. At the draughts of D4 -D6, the floating dock tilts to the starboard due to the retained ballast water in Tank No. 16. The tilting to the fore is more significant than Cases 2 and 3 because the location of Tank No. 16 is farther away from the centre of the floating dock.

Fig. 21 shows the ballast water distributions at different draughts in Case 5. The pumps of Tanks No. 16, 17 and 18 are assumed to be malfunctioning. This case corresponds to the pump failure in a real floating dock [35], where one pump is used to de-ballast the water in three tanks from the port to the starboard. The present case represents the most severe condition where the amount of ballast water in the three tanks is retained during the entire vessel-docking operation. Fig. 22 shows the comparisons of the four draughts

Draught	Ballast water mass [g]					
D1	③ 3791	⑥ 5254	⑨ 5380	⑫ 4352	⑮ 3654	⑱ 3856
	② 4143	⑤ 4537	⑧ 3691	⑪ 4214	⑭ 4672	⑰ 3833
	① 3538	④ 5372	⑦ 5501	⑩ 5104	⑬ 5600	⑯ 3831
D2	③ 0	⑥ 5254	⑨ 5380	⑫ 4352	⑮ 3654	⑱ 0
	② 4143	⑤ 4537	⑧ 3691	⑪ 4214	⑭ 4672	⑰ 3833
	① 0	④ 5372	⑦ 5501	⑩ 5104	⑬ 5600	⑯ 0
D3	③ 0	⑥ 0	⑨ 5380	⑫ 4352	⑮ 0	⑱ 0
	② 4143	⑤ 4537	⑧ 3691	⑪ 4214	⑭ 4672	⑰ 3833
	① 0	④ 0	⑦ 5501	⑩ 5104	⑬ 0	⑯ 0
D4	③ 0	⑥ 0	⑨ 0	⑫ 0	⑮ 0	⑱ 0
	② 4143	⑤ 4537	⑧ 3691	⑪ 4214	⑭ 4672	⑰ 3833
	① 0	④ 0	⑦ 0	⑩ 0	⑬ 0	⑯ 0
D5	③ 0	⑥ 0	⑨ 0	⑫ 0	⑮ 0	⑱ 0
	② 0	⑤ 0	⑧ 3691	⑪ 4214	⑭ 0	⑰ 0
	① 0	④ 0	⑦ 0	⑩ 0	⑬ 0	⑯ 0
D6	③ 0	⑥ 0	⑨ 0	⑫ 0	⑮ 0	⑱ 0
	② 0	⑤ 0	⑧ 0	⑪ 0	⑭ 0	⑰ 0
	① 0	④ 0	⑦ 0	⑩ 0	⑬ 0	⑯ 0

Fig. 8. Ballast water distributions at different draughts in Case 1.
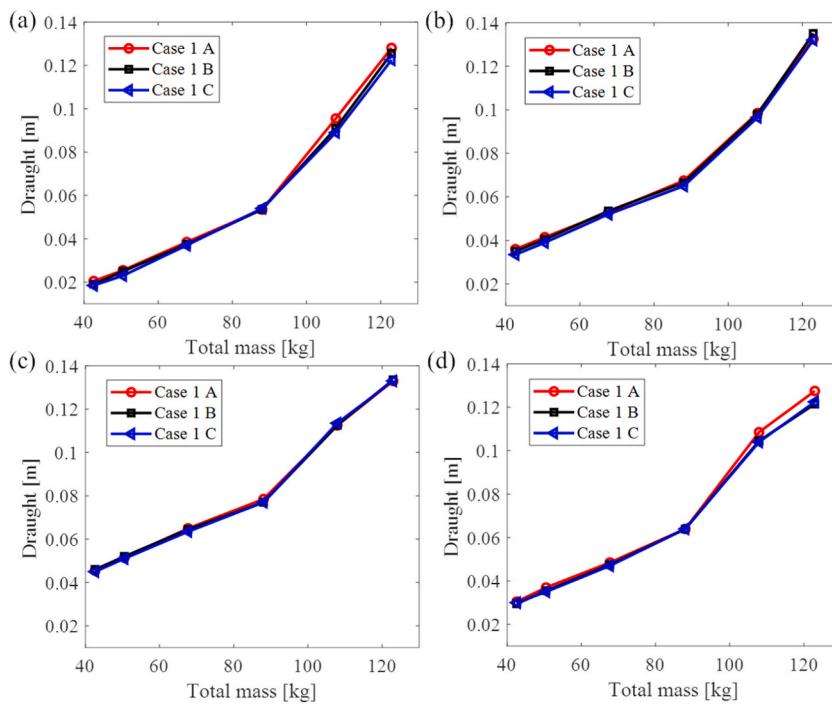
Fig. 9. Draughts of the four draught meters (a) (b) (c) (d) from three repeatable experiments for Case 1.
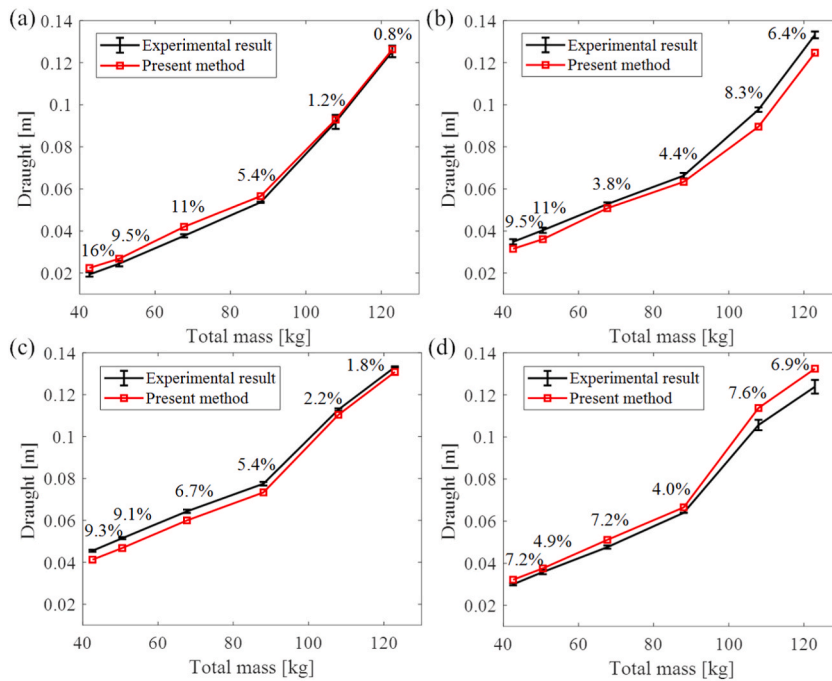
Fig. 10. Comparisons of the four draughts (a) (b) (c) (d) between the experimental results and the numerical predictions for Case 1.

between the experimental results and the numerical predictions for Case 5. Similar to Cases 1–4, a good agreement is obtained with the maximum relative error of 16 %. The entire vessel-docking operation is shown in Fig. 23. The visualizations show that the pontoon deck of the floating dock can successfully emerge from water at the severe condition of pump failure if a well-designed ballast plan is adopted.

4. Validation using field test measurement

4.1. Specifications of the full-scale floating dock and numerical modelling

Fig. 24 shows the setup of field test measurements in the shipyard of Myklebust Verft AS [4]. The details of the floating dock and the docked fjord ferry are given in Table 3. There are 18 ballast tanks installed inside the floating dock, where the details of the ballast tanks can be referred to Wen et al. [35]. The draughts of the floating dock at four draught meters and the ballast water levels in 18 tanks were measured through the initially installed devices of the floating dock. The deflection of the floating dock was measured using a Lecia TCRP1201 syrveying total station and seven optical mirrors installed on the top of the port wing wall. The locations of seven optical mirrors, which correspond to seven measured locations, are shown in Fig. 25. Table 4 lists these positions in the global co-ordinate system.

Two field tests were conducted in July 2023. Figs. 26 and 27 show the time histories of the averaged water levels in Tank Sets No.01-06 in the field tests 1 and 2, respectively. The operations of the ballast water system in the field test 1 are described as follows.

(1) Tank Sets 1 and 6 start de-ballasting at 300s and stop de-ballasting at 1300s.
(2) Tanks Sets 2 and 5 start de-ballasting at 1040s and stop de-ballasting at 1300s.
(3) Tank Sets 3 and 4 start ballasting at 1300s and stop ballasting at 1515s.
(4) Tank Sets 3 and 4 start de-ballasting at 1515s and stop de-ballasting at 1850s.
(5) Tank Sets 1, 2, 5 and 6 start ballasting at 1850s and stop ballasting at 3465s.

The above operation aims to adjust the ballast water distributions, and thereby change the bending deformation of the floating dock, which can be measured using the total station. During the operation, the on-board docked vessel remained entirely out of water.

The operations of the ballast system in the field test 2 are given as follows.

(1) Tank Sets 1 and 6 start de-ballasting at 1413s and stop ballasting at 2439s.
(2) Tanks Sets 3 and 4 start de-ballasting at 2439s and stop de-ballasting at 3912s.
(3) Tank Sets 1 and 6 start ballasting at 4089s and stop ballasting at 5784s.
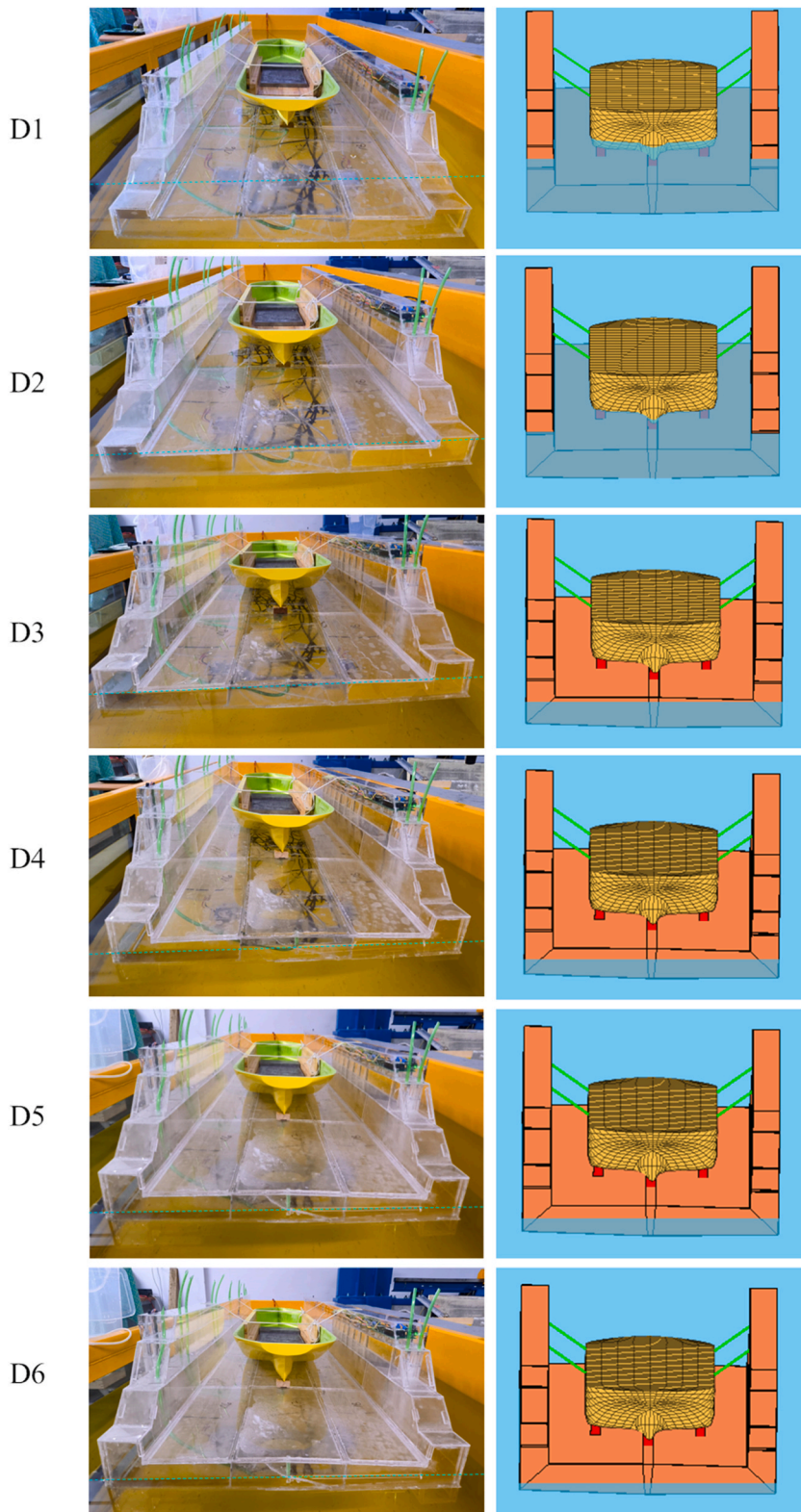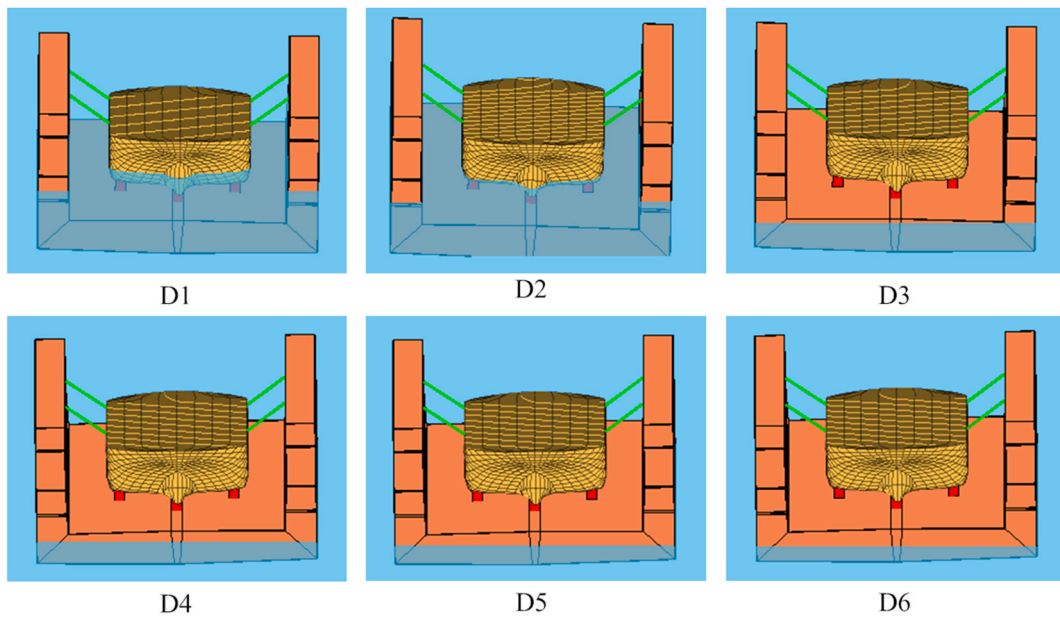(4) Tank Sets 5 and 6 start de-ballasting at 6034s and stop de-ballasting at 6601s.

Fig. 11. Comparisons of the floating dock's and docked vessel's positions at various total masses between the experimental results and the present numerical results for Case 1.

Draught	Ballast water mass [g]					
D1	③ 4512	⑥ 5183	⑨ 5647	⑫ 5412	⑮ 5203	⑱ 4149
	② 4160	⑤ 4565	⑧ 4358	⑪ 3022	⑭ 4655	⑰ 3982
	① 4838	④ 5314	⑦ 5624	⑩ 5723	⑬ 5222	⑯ 4516
D2	③ 0	⑥ 5183	⑨ 5647	⑫ 5412	⑮ 5203	⑱ 0
	② 4160	⑤ 4565	⑧ 4358	⑪ 3022	⑭ 4655	⑰ 3982
	① 0	④ 5314	⑦ 5624	⑩ 5723	⑬ 5222	⑯ 0
D3	③ 0	⑥ 0	⑨ 5647	⑫ 5412	⑮ 0	⑱ 0
	② 4160	⑤ 4565	⑧ 4358	⑪ 3022	⑭ 4655	⑰ 3982
	① 0	④ 0	⑦ 5624	⑩ 5723	⑬ 0	⑯ 0
D4	③ 0	⑥ 0	⑨ 0	⑫ 0	⑮ 0	⑱ 0
	② 4160	⑤ 4565	⑧ 4358	⑪ 0	⑭ 4655	⑰ 3982
	① 0	④ 0	⑦ 0	⑩ 5723	⑬ 0	⑯ 0
D5	③ 0	⑥ 0	⑨ 0	⑫ 0	⑮ 0	⑱ 0
	② 0	⑤ 4565	⑧ 4358	⑪ 0	⑭ 4655	⑰ 0
	① 0	④ 0	⑦ 0	⑩ 5723	⑬ 0	⑯ 0
D6	③ 0	⑥ 0	⑨ 0	⑫ 0	⑮ 0	⑱ 0
	② 0	⑤ 0	⑧ 0	⑪ 0	⑭ 0	⑰ 0
	① 0	④ 0	⑦ 0	⑩ 5723	⑬ 0	⑯ 0

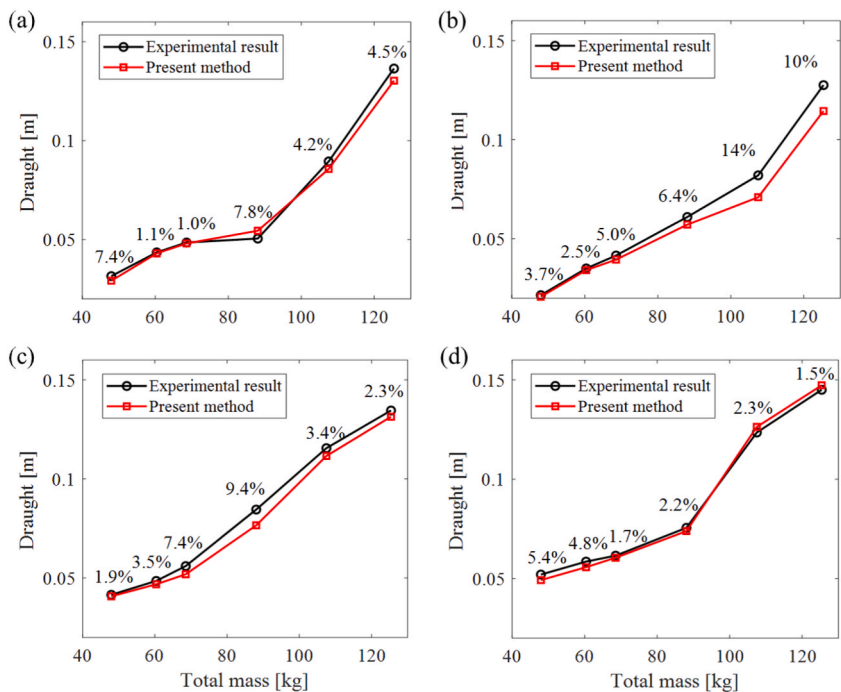**Fig. 12.** Ballast water distributions at different draughts in Case 2.
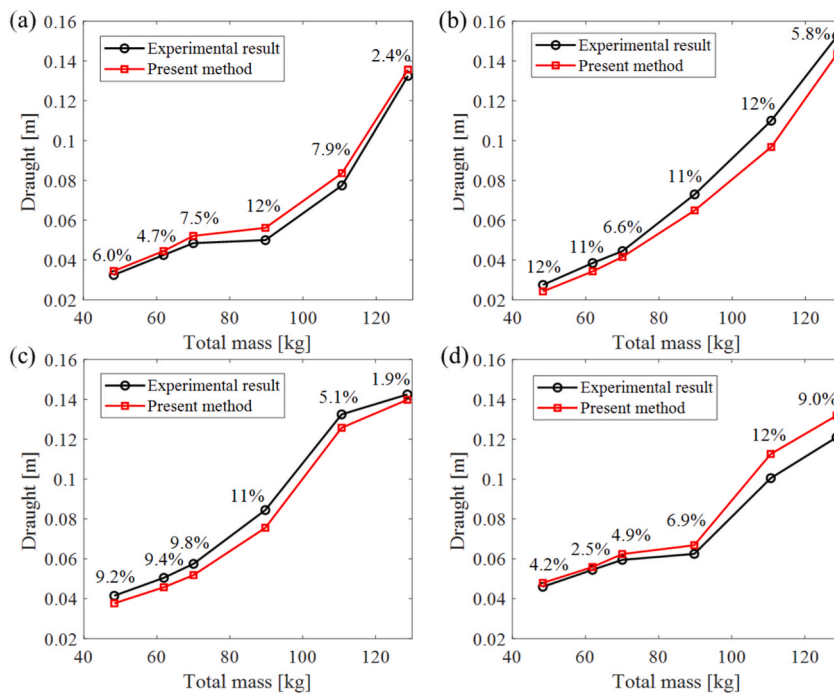
Fig. 13. Comparisons of the four draughts (a) (b) (c) (d) between the experimental results and the numerical predictions for Case 2.

Fig. 14. Floating dock's and docked vessel's positions at various total masses for Case 2.

Fig. 15. Ballast water distributions at different draughts in Case 3.

Fig. 16. Comparisons of the four draughts (a) (b) (c) (d) between the experimental results and the numerical predictions for Case 3.
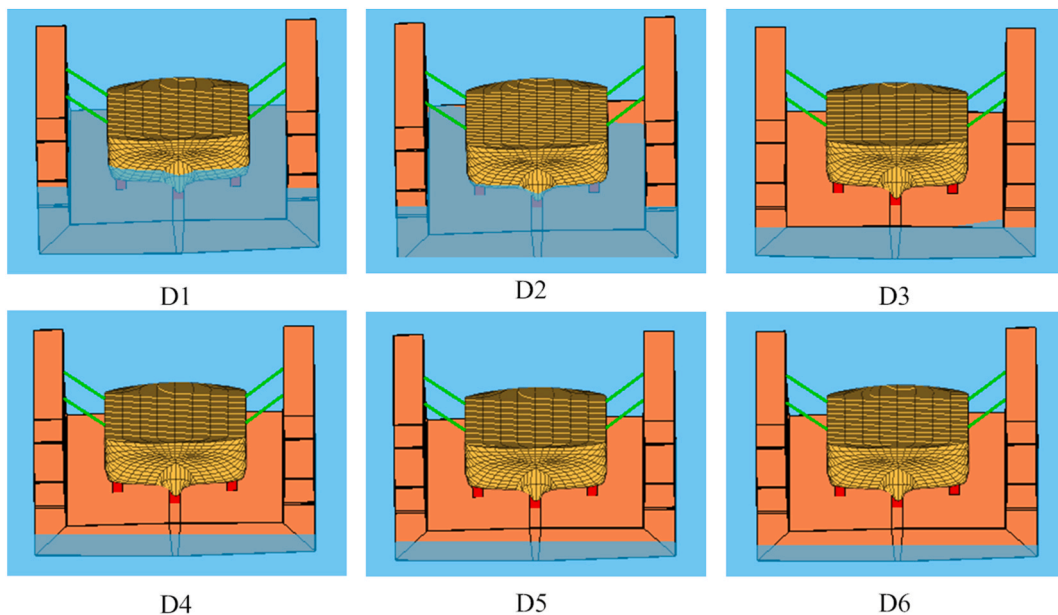

Fig. 17. Floating dock's and docked vessel's positions at various total masses for Case 3.

(5) Tank Sets 5 and 6 start ballasting at 6911s and stop ballasting at 8104s.

The deflection of the floating dock top wing was measured using the optical measurement system. However, the deflection of the floating dock cannot be accurately calculated because we lacked the exact weight distribution of the docked vessel. The deflection change between two positions can be precisely predicted because it only depends on the change in the ballast water distribution. Therefore, in the present study, three positions of the floating dock are chosen for measurement, and the deflection change between these positions is compared with the predictions of the developed numerical method.

Draught	Ballast water mass [g]					
D1	③ 4482	⑥ 4010	⑨ 4128	⑫ 4707	⑮ 4501	⑱ 4939
	② 4263	⑤ 4537	⑧ 4708	⑪ 4235	⑭ 4672	⑰ 4111
	① 4439	④ 5933	⑦ 4967	⑩ 5249	⑬ 4468	⑯ 4538
D2	③ 0	⑥ 4010	⑨ 4128	⑫ 4707	⑮ 4501	⑱ 0
	② 4263	⑤ 4537	⑧ 4708	⑪ 4235	⑭ 4672	⑰ 4111
	① 0	④ 5933	⑦ 4967	⑩ 5249	⑬ 0	⑯ 4538
D3	③ 0	⑥ 0	⑨ 4128	⑫ 4707	⑮ 0	⑱ 0
	② 4263	⑤ 4537	⑧ 4708	⑪ 4235	⑭ 4672	⑰ 4111
	① 0	④ 0	⑦ 4967	⑩ 0	⑬ 0	⑯ 4538
D4	③ 0	⑥ 0	⑨ 0	⑫ 0	⑮ 0	⑱ 0
	② 4263	⑤ 4537	⑧ 4708	⑪ 4235	⑭ 4672	⑰ 0
	① 0	④ 0	⑦ 0	⑩ 0	⑬ 0	⑯ 4538
D5	③ 0	⑥ 0	⑨ 0	⑫ 0	⑮ 0	⑱ 0
	② 0	⑤ 4537	⑧ 4708	⑪ 4235	⑭ 0	⑰ 0
	① 0	④ 0	⑦ 0	⑩ 0	⑬ 0	⑯ 4538
D6	③ 0	⑥ 0	⑨ 0	⑫ 0	⑮ 0	⑱ 0
	② 0	⑤ 0	⑧ 0	⑪ 0	⑭ 0	⑰ 0
	① 0	④ 0	⑦ 0	⑩ 0	⑬ 0	⑯ 4538

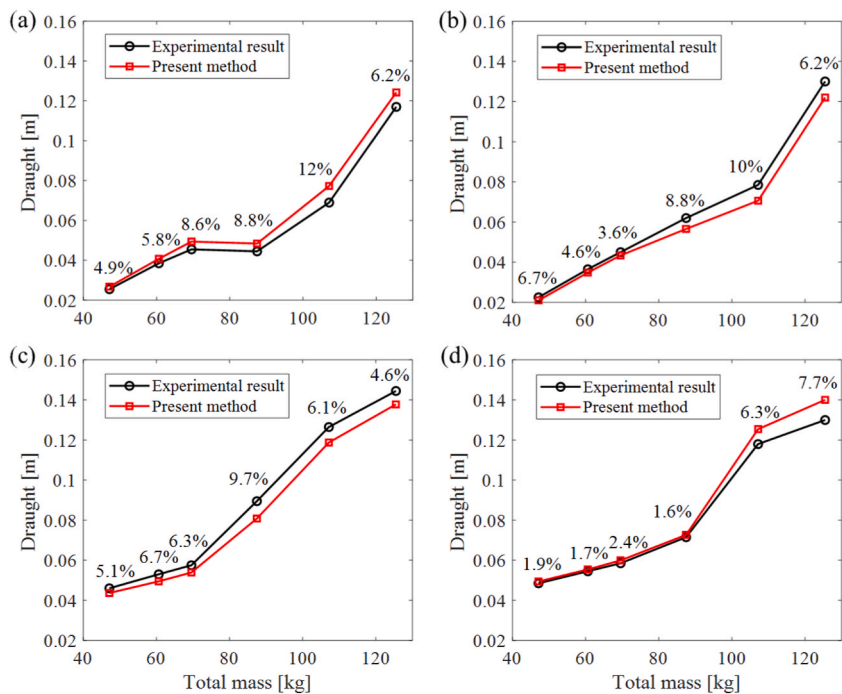**Fig. 18.** Ballast water distributions at different draughts in Case 4.

Fig. 19. Comparisons of the four draughts (a) (b) (c) (d) between the experimental results and the numerical predictions for Case 4.
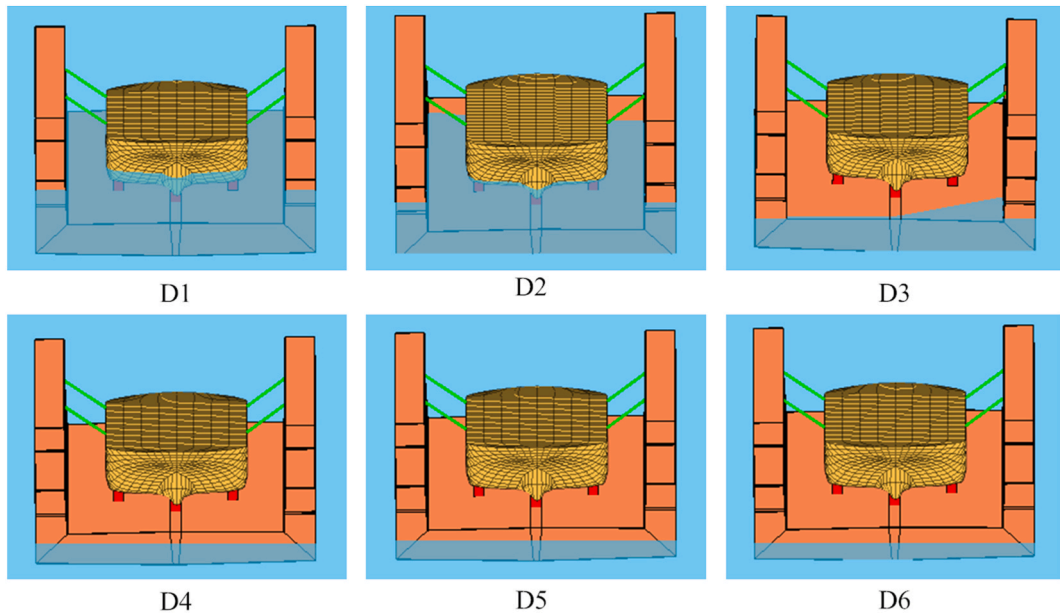
Fig. 20. Floating dock's and docked vessel's positions at various total masses for Case 4.

Draught	Ballast water mass [g]					
D1	③ 4459	⑥ 5019	⑨ 4464	⑫ 5048	⑮ 4785	⑱ 4696
	② 4163	⑤ 4496	⑧ 4226	⑪ 4578	⑭ 4519	⑰ 4080
	① 5247	④ 6085	⑦ 5566	⑩ 5232	⑬ 4985	⑯ 4821
D2	③ 4459	⑥ 0	⑨ 4464	⑫ 5048	⑮ 0	⑱ 4696
	② 4163	⑤ 4496	⑧ 4226	⑪ 4578	⑭ 4519	⑰ 4080
	① 5247	④ 0	⑦ 5566	⑩ 5232	⑬ 0	⑯ 4821
D3	③ 4459	⑥ 0	⑨ 0	⑫ 0	⑮ 0	⑱ 4696
	② 4163	⑤ 4496	⑧ 4226	⑪ 4578	⑭ 4519	⑰ 4080
	① 5247	④ 0	⑦ 0	⑩ 0	⑬ 0	⑯ 4821
D4	③ 0	⑥ 0	⑨ 0	⑫ 0	⑮ 0	⑱ 4696
	② 4163	⑤ 4496	⑧ 4226	⑪ 0	⑭ 0	⑰ 4080
	① 0	④ 0	⑦ 0	⑩ 0	⑬ 0	⑯ 4821
D5	③ 0	⑥ 0	⑨ 0	⑫ 0	⑮ 0	⑱ 4696
	② 0	⑤ 0	⑧ 0	⑪ 0	⑭ 0	⑰ 4080
	① 0	④ 0	⑦ 0	⑩ 0	⑬ 0	⑯ 4821

Fig. 21. Ballast water distributions at different draughts in Case 5.

In the present numerical study, the floating dock position free of loads is selected as the reference position. The restoring hydrostatic coefficients of the full scale model of the floating dock with a vessel on board were given by Wen et al. [35]. The deflections of the floating dock at Positions A, B and C are calculated based on the bending model of Equations (14) and (15) in Section 2.3 and the static analysis model based on the models in Sections 2.1 and 2.2.

4.2. Comparison between the field tests and numerical results

Table 5 shows the details of three measurements, where the time instant of Locations A and C are changed with a small time shift of
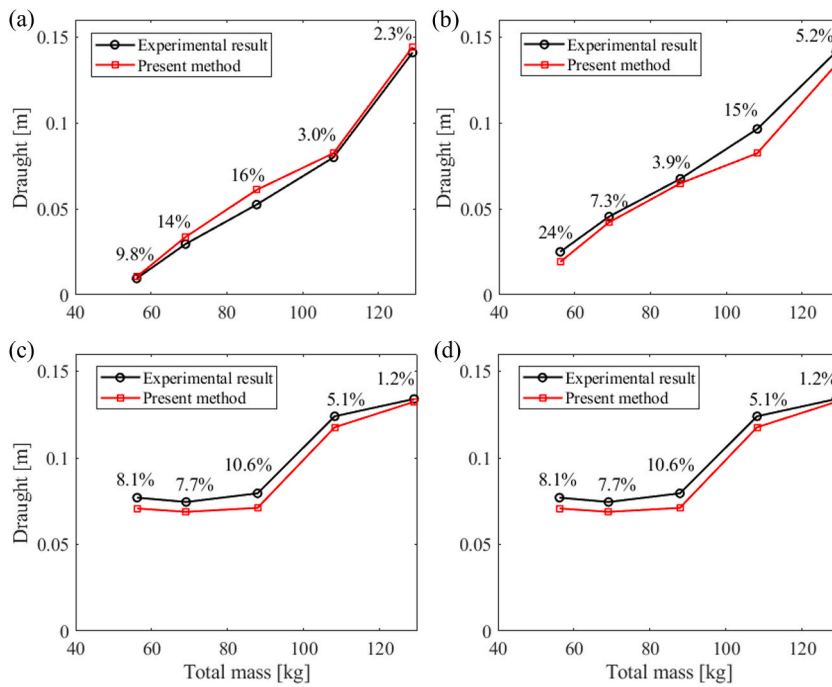
Fig. 22. Comparisons of the four draughts (a) (b) (c) (d) between the experimental results and the numerical predictions for Case 5.
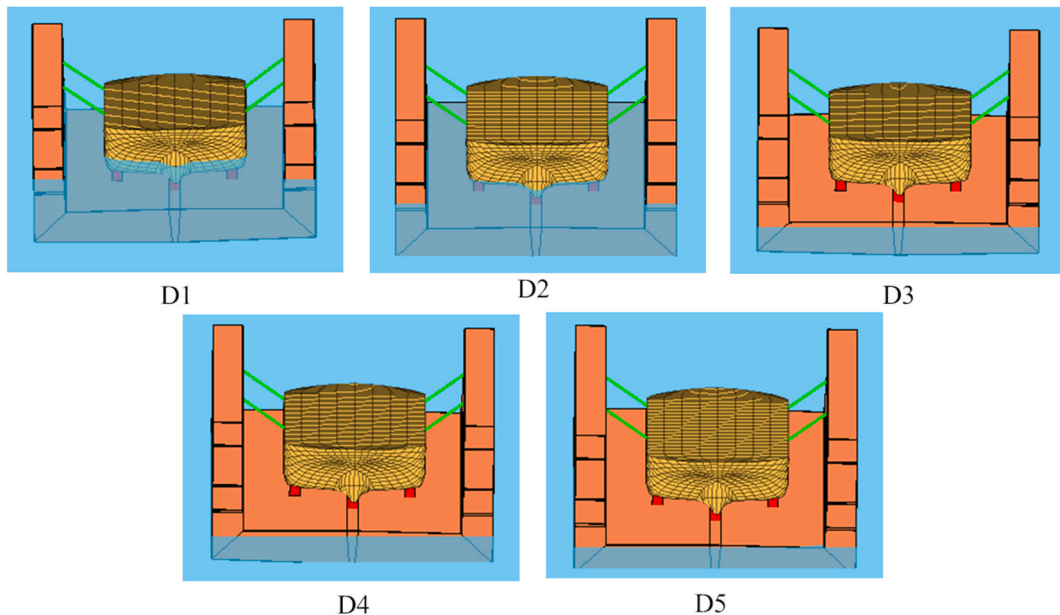

Fig. 23. Floating dock's and docked vessel's positions at various total masses for Case 5.

60s. These repeatable measurements of the deflection changes of the floating dock from A to B and from B to C are shown in Figs. 28 and 29, respectively. As can be seen from the two figures, a good agreement is achieved within the three measurements, which indicates the stability of the optical measurement in the present study.

Fig. 30 shows the comparison of the deflection change from Position A to B between the experimental result and the prediction of the present numerical method. As the floating dock moves from Position A to B, it experiences a decrease in hogging, resulting in a sagging distribution in the deflection change. The results obtained from the present numerical method closely match those from the experiments, exhibiting a maximum relative error of 8.6 %. Fig. 31 shows the comparison of the deflection change from Position B to C between the experimental result and the prediction of the present numerical method. The deflection change of the floating dock shows

Fig. 24. Setup of field test measurement.

Table 3

Floating dock and docked vessel specifications in field test measurement.

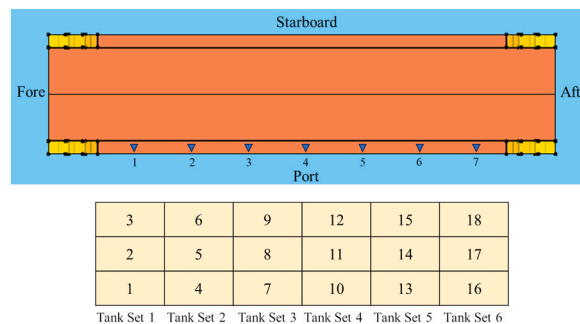| Description	Floating dock	Docked vessel
Dimensions, $L \times B \times H$ [m]	$168.48 \times 39.8 \times 18.2$	$84 \times 17 \times 11.05$
Mass [kg]	5.1782×10^6	1.9872×10^6
Initial CoG, $(X_{CG0}, Y_{CG0}, Z_{CG0})$ [m]	$(-0.4349, 0.0929, 5.4967)$	$(-0.72, 0.0, 8.5)$

Fig. 25. Optical mirror locations at the top of the port wing wall and the description of Tank Sets 1–6.

Table 4

Optical mirror locations in the global coordinate system.

Description	1	2	3	4	5	6	7
x [m]	−68.04	−45.3	−23.04	0.94	23.38	45.69	68.01

hogging in this case. The predictions of the present numerical method are also consistent with the experimental results, with a maximum relative error of 10 %. The good agreement of the deflection change with the experimental measurement indicates the accuracy of the present numerical method.

Figs. 32 and 33 show the comparison of the deflection changes from Positions A to B and from Position A to C between the experimental result and the prediction of the present numerical method, respectively. A maximum relative error of 11 % is observed. The agreement between the experiments and the numerical method is acceptable.
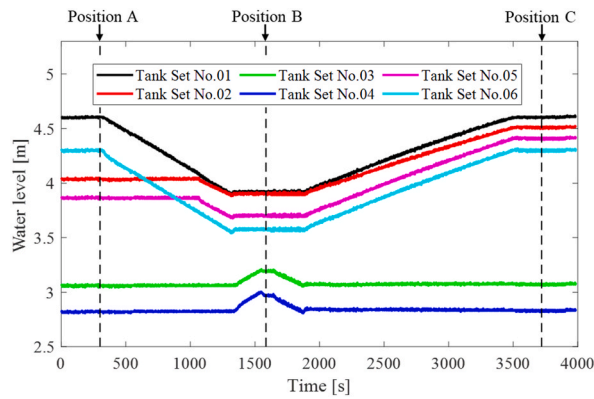
Fig. 26. Time histories of the averaged water levels in Tank Sets No.01–06 in the field test 1.
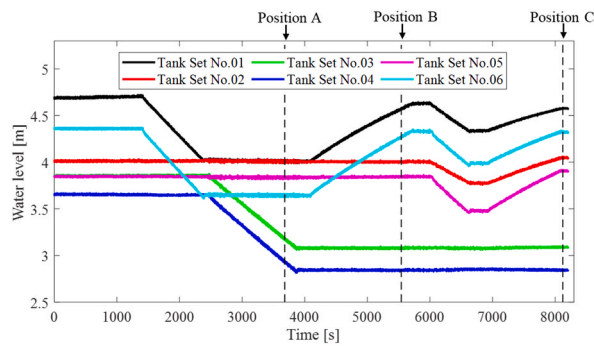

Fig. 27. Time histories of the water levels in Tanks No.01–06 in the field test 2.

Table 5
Details of three measurements.

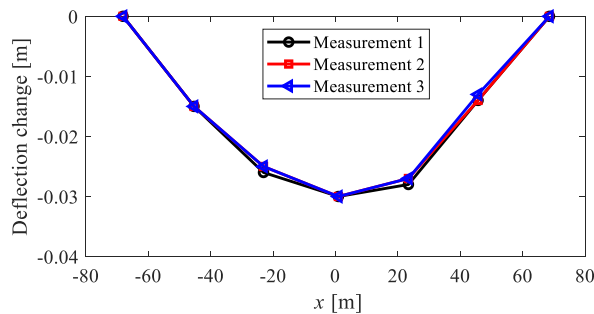|	Position A [s]	Position B [s]	Position C [s]
Measurement 1	240	1585	3660
Measurement 2	300	1585	3720
Measurement 3	360	1585	3780

Fig. 28. Deflection changes of the floating dock from Position A to B in three measurements in the field test 1.

5. Conclusion

A comparative study of numerical modelling and experimental investigation for vessel-docking operations with a vessel on board is performed in the present study. The model-scale experiments and field test measurements are conducted on floating docks with vessels on board. The present numerical method presents a static analysis of the floating dock during vessel-docking operations, providing the
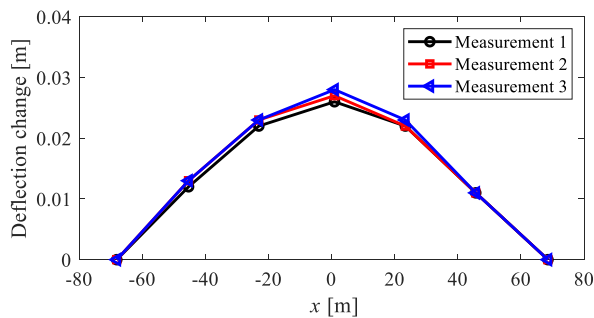
Fig. 29. Deflection changes of the floating dock from Position B to C in three measurements in the field test 1.
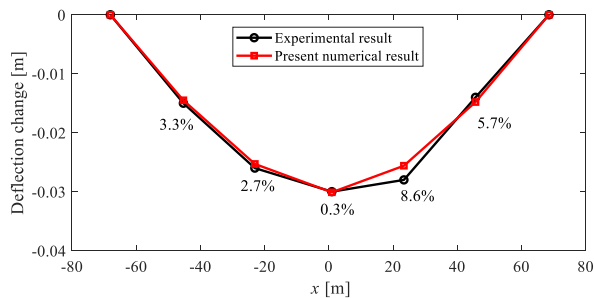

Fig. 30. Comparison of the deflection change from Position A to B between the experimental result and the prediction of the present numerical method in the field test 1.

Fig. 31. Comparison of the deflection change from Position B to C between the experimental result and the prediction of the present numerical method in the field test 1.

Fig. 32. Comparison of the deflection change from Position A to B between the experimental result and the prediction of the present numerical method in the field test 2.
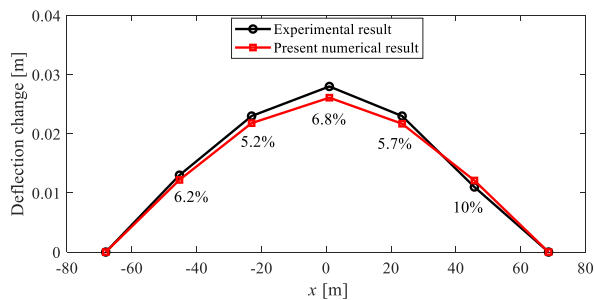
Fig. 33. Comparison of the deflection change from Position A to C between the experimental result and the prediction of the present numerical method in the field test 2.
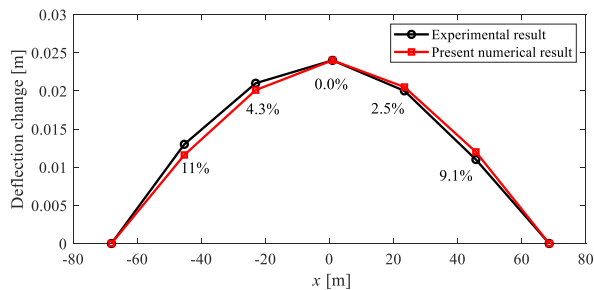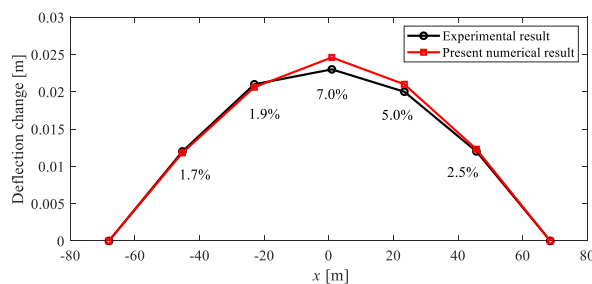
draughts and bending deformation of the floating dock under a specific ballast water distribution. The effect of the vessel on board on the docking process of the floating dock is involved in this study. The comparative study of the numerical predictions and the experimental measurements are summarized as follows:

- The comparison of the model-scale results, including the draught measurement and photographs of floating dock positions, validates the present numerical method for simulating vessel-docking operations.
- Successful de-ballasting operations on a model-scale floating dock are achievable with a well-designed ballast plan, even in the event of one to three pump failures.
- The comparison of the deflection change in the full-scale floating dock between the experimental and numerical results proves the accuracy of the present bending model.

Therefore, the validated numerical model, tested on both model-scale and full-scale docks, can serve as a reliable foundation for creating a digital twin for floating docks in shipyards.

CRediT authorship contribution statement

Xueliang Wen: Writing – review & editing, Writing – original draft, Visualization, Validation, Software, Methodology, Investigation, Formal analysis, Data curation, Conceptualization. **Jianan Zhang:** Writing – review & editing, Validation, Software, Methodology, Investigation, Formal analysis, Data curation, Conceptualization. **Muk Chen Ong:** Writing – review & editing, Supervision, Resources, Project administration, Methodology, Investigation, Funding acquisition, Formal analysis, Conceptualization. **Aleksander Kniat:** Writing – review & editing, Resources, Project administration, Methodology, Investigation, Funding acquisition, Conceptualization.

Declaration of competing interest

The authors declare that they have no known competing financial interests or personal relationships that could have appeared to influence the work reported in this paper.

Data availability

Data will be made available on request.

Acknowledgement

References

[1] Warnke HJ. The construction and testing of a 33,000-Ton (M) lift floating dry dock. Marine Technology and SNAME News 1975;12(2):177–89. https://doi.org/10.5957/mt1.1975.12.2.177.

[2] Sadeghi K, Derki A, Shlash A. Dry docks: overview of design and construction. Acad Res Int 2018;9(1).

[3] Sullivan AA. Photograph of dry dock one, looking out to Boston harbor. Available from, https://www.nps.gov/places/cny-dry-dock-1.htm. [Accessed 20 January 2024].

[4] Myklebust Vert AS. A flexible yard. Available from, https://www.myklebustverft.no/#introfilm. [Accessed 23 June 2024].

[5] David M. Vessels and ballast water. Global maritime transport and ballast water management: issues and solutions. New York, USA: Springer; 2015. p. 13–34.

[6] De Baere K, Verstraelen H, Rigo P, Van Passel S, Lenaerts S, Potters G. Reducing the cost of ballast tank corrosion: an economic modeling approach. Mar Struct 2013;32:136–52. https://doi.org/10.1016/j.marstruc.2012.10.009.

[7] Gul M, Celik E, Akyuz E. A hybrid risk-based approach for maritime applications: the case of ballast tank maintenance. Hum Ecol Risk Assess 2017;23(6): 1389–403. https://doi.org/10.1080/10807039.2017.1317204.

[8] Kimera D, Nangolo FN. Predictive maintenance for ballast pumps on ship repair yards via machine learning. Transport Eng 2020;2:100020. https://doi.org/10.1016/j.treng.2020.100020.

[9] National Transportation Safety Board. Dockside capsizing and sinking of towing vessel invader and dry dock #3. Available from, https://www.ntsb.gov/investigations/AccidentReports/Reports/MAB1316.pdf. [Accessed 18 March 2012].

[10] Rainsford S. Russian aircraft carrier Admiral Kuznetsov damaged by crane. Available from, https://www.bbc.com/news/world-europe-46030113. [Accessed 30 October 2018].

[11] Wang Z, Qian Z. Effects of concentration and size of silt particles on the performance of a double-suction centrifugal pump. Energy 2017;123:36–46. https://doi.org/10.1016/j.energy.2017.01.142.

[12] Retired Felixstowe Dockers. Floating dock with 2 ships inside broke in two, crane collapsed, ships taking on water. Available from, https://www.felixstowedocker.com/2019/04/floating-dock-with-2-ships-inside-broke.html; 2019. Apr. 2019.

[13] Insurance Marine News. Floating docks and their operational hazards. Available from, https://insurancemarinenews.com/insurance-marine-news/floating-docks-and-their-operational-hazards/. [Accessed 20 August 2019].

[14] Brewer T, Knight D, Noiray G, Naik H. Digital twin technology in the field reclaims offshore resources. Houston, Texas, USA. In the offshore Technology conference. 2019. https://doi.org/10.4043/29231-MS.

[15] Wang M, Wang C, Hnydiuk-Stefan A, Feng S, Atilla I, Li Z. Recent progress on reliability analysis of offshore wind turbine support structures considering digital twin solutions. Ocean Eng 2021;232:109168. https://doi.org/10.1016/j.oceaneng.2021.109168.

[16] Liu M, Fang S, Dong H, Xu C. Review of digital twin about concepts, technologies, and industrial applications. J Manuf Syst 2021;58:346–61. https://doi.org/10.1016/j.jmsy.2020.06.017.

[17] West S, Stoll O, Meierhofer J, Züst S. Digital twin providing new opportunities for value co-creation through supporting decision-making. Appl Sci 2021;11(9): 3750. https://doi.org/10.3390/app11093750.

[18] Tao F, Zhang H, Liu A, Nee AY. Digital twin in industry: state-of-the-art. IEEE Trans Ind Inf 2018;15(4):2405–15. https://doi.org/10.1109/TII.2018.2873186.

[19] Korotaev VV, Pantiushin AV, Serikova MG, Anisimov AG. Deflection measuring system for floating dry docks. Ocean Eng 2016;117:39–44. https://doi.org/10.1016/j.oceaneng.2016.03.012.

[20] Yang G, Liang H, Wu C. Deflection and inclination measuring system for floating dock based on wireless networks. Ocean Eng 2013;69:1–8. https://doi.org/10.1016/j.oceaneng.2013.05.014.

[21] Drwięga K, Gucma L, Gralak R. Method for reserve determination of static and dynamic list of bulk carriers applied to the dynamic under keel clearance system in the port of Świnoujście. Annu Navig 2017;(24):89–102. https://doi.org/10.1515/aon-2017-0007.

[22] Golz M, Boeck F, Ritz S, Holbach G. A ballast system for automated deep-sea ascents. In: The international conference on offshore mechanics and arctic engineering, vol. 49989. Busan, South Korea: American Society of Mechanical Engineers; 2016, V007T06A028. https://doi.org/10.1115/OMAE2016-54841.

[23] Wang G, Pran K, Sagvolden G, Havsgård G, Jensen A, Johnson G, Vohra S. Ship hull structure monitoring using fibre optic sensors. Smart Mater Struct 2001;10 (3):472. https://doi.org/10.1088/0964-1726/10/3/308.

[24] Hsu C-Y, Chiang C-C, Hsieh T-S, Chen T-H, Chen Y-H. A study of strain measurement in cylindrical shells subjected to underwater shock loading using FBG sensors. Optik 2020;217:164701. https://doi.org/10.1016/j.ijleo.2020.164701.

[25] Ma Y, Chen P, Yang C, Cheng Z, Xiao L. Development and experimental validation of an FBG-based substructure cross-sectional load measurement approach for a semi-submersible floating wind turbine. Eng Struct 2024;303:117527. https://doi.org/10.1016/j.engstruct.2024.117527.

[26] Ren L, Li H-N, Zhou J, Li D-S, Sun L. Health monitoring system for offshore platform with fiber Bragg grating sensors. Opt Eng 2006;45(8):84401–9. https://doi.org/10.1117/1.2335858.

[27] Uhlemann TH-J, Schock C, Lehmann C, Freiberger S, Steinhilper R. The digital twin: demonstrating the potential of real time data acquisition in production systems. Procedia Manuf 2017;9:113–20. https://doi.org/10.1016/j.promfg.2017.04.043.

[28] Uhlemann TH-J, Lehmann C, Steinhilper R. The digital twin: realizing the cyber-physical production system for industry 4.0. Procedia Cirp 2017;61:335–40. https://doi.org/10.1016/j.procir.2016.11.152.

[29] Zhang J, Li L, Ong MC, El Beshbichi O, Kniat A. Development of a response assessment tool for a floating dock system. In: ASME 2022 41st international conference on ocean, offshore and arctic engineering, American society of mechanical engineers, vol. 85901; 2022. https://doi.org/10.1115/OMAE2022-78997. V05BT06A014) Hamburg, Germany. June 5–10, 2022.

[30] Zhang J, Wen X, Ong MC. Development of a floating dock numerical model and the ballast water distribution strategy. In: ASME 2023 42nd international conference on ocean, offshore and arctic engineering, vol. 86878. Melbourne, Australia: American Society of Mechanical Engineers; 2023, V005T06A068. https://doi.org/10.1115/OMAE2023-102996. June 11–16, 2023.

[31] Zhang J, Ong MC, Wen X. Dynamic and structural analyses of floating dock operations considering dock-vessel coupling loads. Ocean Eng 2024;118622. https://doi.org/10.1016/j.oceaneng.2024.118622.

[32] Zhang J, Wen X, Kniat A, Ong MC. A comparative analysis of numerically simulated and experimentally measured static responses of a floating dock. Ships Offshore Struct 2024:1–18. https://doi.org/10.1080/17445302.2024.2336670.

[33] Wen X, García Conde A, Zhang J, Ong MC. Numerical study on the automatic ballast control of a floating dock. In: ASME 2023 42nd international conference on ocean, offshore and arctic engineering, vol. 86878. Melbourne, Australia: American Society of Mechanical Engineers; 2023, V005T06A067. https://doi.org/10.1115/OMAE2023-102873. June 11–16, 2023.

[34] Wen X, García Conde A, Zhang J, Ong MC. Dynamic analysis of a floating dock under accidental conditions. Appl Ocean Res 2024;144:103908. https://doi.org/10.1016/j.apor.2024.103908.

[35] Wen X, Zhang J, García Conde A, Ong MC. Numerical study on the automatic ballast control of a floating dock. J Offshore Mech Arctic Eng 2024;146(4). https://doi.org/10.1115/1.4064014.